Plant Pathol. J. 41(5) : 682-698 (2025)
https://doi.org/10.5423/PPJ.FT.08.2025.0107
eISSN 2093-9280

Research Article Open Access Fast Track

The Plant Pathology Journal

Comparative Genomics Reveals Conserved Ophiobolin Biosynthetic Gene Cluster and Necrotrophic Adaptation in *Bipolaris oryzae*

Yoeguang Hue[1†], Yebin Nam[1†], Byungheon Choi[2], Seoyeon Kim[1,3], Seol-Hwa Jang[1], Hyunjung Chung[4], Sook-Young Park[1,3,5], and Ki-Tae Kim [1,5*]

[1]*Department of Plant Medicine, Sunchon National University, Suncheon 57922, Korea*
[2]*Department of Artificial Intelligence Engineering, Sunchon National University, Suncheon 57922, Korea*
[3]*Interdisciplinary Program in IT-Bio Convergence System (BK21 plus), Sunchon National University, Suncheon 57922, Korea*
[4]*Department of Crop Sciences, National Institute of Crop Science, Rural Development Administration, Wanju 55365, Korea*
[5]*Department of Agricultural Life Science, Sunchon National University, Suncheon 57922, Korea*

(Received on August 18, 2025; Revised on August 29, 2025; Accepted on September 1, 2025)

***Bipolaris oryzae*, the causal agent of rice brown spot, is a necrotrophic fungus that produces phytotoxic secondary metabolites, yet its genomic basis of pathogenicity remains incompletely defined. We sequenced six South Korean *B. oryzae* isolates and analyzed them together with publicly available genomes from *Bipolaris* and related Pleosporaceae, covering 37 *Bipolaris* isolates across eight species. Phylogenomics based on single-copy orthologs confirmed the monophyly of *Bipolaris* and resolved *B. oryzae* as a distinct lineage. Comparative analyses showed that *B. oryzae* has a moderately reduced secretome and fewer candidate pathogenicity gene families relative to *B. maydis* and *B. sorokiniana*, while retaining a conserved core enriched in carbohydrate and amino acid metabolism. We identified 48 secondary metabolite biosynthetic gene clusters in *B. oryzae* F1253 and, critically, localized the ophiobolin biosynthetic gene cluster to pseudochromosome 2. The cluster contains conserved core genes, *oblA* to *oblD*, which are broadly retained across *Bipolaris*, and exhibits interspecies variation in synteny and copy number associated with repeat element insertions. These findings reveal the genomic architecture underlying metabolic specialization and toxin biosynthesis in *B. oryzae*. They also provide actionable targets and markers for management, including diagnostics for *oblA* to *oblD*, screening of rice germplasm for ophiobolin tolerance, and RNAi-based suppression of ophiobolin biosynthesis under climate-related stress.**

Keywords **:** *Bipolaris oryzae*, brown spot, *Cochliobolus miyabeanus*, genome, rice

[†]These authors contributed equally to this work.
*Corresponding author.
Phone) +82-61-750-5193, FAX) +82-61-750-3208
E-mail) kitaekim@scnu.ac.kr
ORCID
Ki-Tae Kim
https://orcid.org/0000-0002-8249-5283

Handling Editor : Junhyun Jeon

Bipolaris oryzae (teleomorph *Cochliobolus miyabeanus*) is a filamentous ascomycete fungus responsible for brown spot disease in rice (*Oryza sativa*), a significant foliar disease affecting global rice production. The pathogen is classified as a necrotrophic and infects leaves, sheaths, and grains, producing characteristic brown lesions with gray or whitish centers that reduce photosynthesis capacity and grain development (Sunder et al., 2014). In addition to rice, *B. oryzae* has a broad host range among grasses, including wild species and weeds, and is often seed-borne, with infection rates reaching up to 76% in heavily infested fields (Kaboré et al., 2025; Ouedraogo et al., 2016). Brown spot

epidemics have historically resulted in devastating consequences, most notably during the Bengal Famine of 1943, and continue to cause chronic yield losses in many rice-producing regions (Dasgupta, 1984).

Environmental stress conditions, particularly drought and nutrient deficiency, are known to exacerbate brown spot severity. Drought stress weakens host defense mechanisms and enhances susceptibility to *B. oryzae*, and the disease is often used as an indicator of abiotic stress in the field (Das et al., 2024). Recent studies suggest that climate change is altering the epidemiology of rice diseases, including brown spot (Hue et al., 2025). Rising global temperatures and increasing drought frequency are creating favorable conditions for the resurgence of *B. oryzae*, especially in upland and rainfed rice systems (Sunder et al., 2014). Hue et al. (2025) report that brown spot incidence is increasing in parts of South Korea due to climate-induced changes in precipitation and temperature patterns, emphasizing the pathogen's potential threat in the context of global climate change.

In contrast to the extensive historical and epidemiological knowledge of brown spot, genomic insights into *B. oryzae* have until recently remained limited. Early molecular studies documented high genetic diversity within *B. oryzae* populations and the absence of a strict clonal lineage structure, suggesting frequent recombination or gene flow among strains (Kaboré et al., 2022). However, genomic resources have lagged behind, with only three genome assemblies available prior to this study (Castell-Miller et al., 2016; Condon et al., 2013; Liu et al., 2024). The first reference genome of *B. oryzae* (isolate ATCC 44560) was sequenced as part of a broader comparative genomics initiative that also included multiple related *Bipolaris* species, revealing the absence of host-specific toxin genes and highlighting the role of general virulence factors (Condon et al., 2013). These include small-secreted proteins, cell wall-degrading enzymes, and phytotoxic secondary metabolites such as ophiobolin, which disrupt host cell membranes and suppress plant immune responses (Xiao et al., 1991).

To address these gaps in genomic knowledge, we sequenced the genomes of six *B. oryzae* isolates (F1248, F1253, F1305, F1318, F1371, and F1409) collected from rice fields in South Korea and integrated them with three publicly available *B. oryzae* genomes (ATCC 44560, Bo-1, and TG12bL2) and genomes of other *Bipolaris* species. Using a comparative genomics approach, we characterized genome architecture, gene family evolution, secondary metabolite biosynthetic gene clusters (SMBGCs), and phylogenomic relationships. Our study reveals both conserved and lineage-specific genomic features, highlights the genomic diversity within *B. oryzae*, and provides new insight into the evolution of pathogenicity and secondary metabolism in *Bipolaris* fungi. These findings offer a valuable foundation for future research into fungal adaptation, host interaction, and disease management in the face of climate variability.

Materials and Methods

Sample collection and fungal isolation. Six *B. oryzae* isolates were obtained from symptomatic rice plants in South Korea and are publicly available under BioProject accession PRJNA1232948 in the National Center for Biotechnology Information (NCBI) database (Kim et al., 2025). To isolate the pathogen, tissue samples (5 × 5 mm) were excised from the interface between healthy and diseased regions of brown spot lesions. The samples were surface sterilized by immersion in 100% ethanol for 1 min followed by 1% sodium hypochlorite (NaOCl) for another minute. Subsequently, the tissues were rinsed three times in sterile distilled water for 30 s each and blotted dry under aseptic conditions. Sterilized samples were plated on 1.5% water agar (15 g agar/L) supplemented with streptomycin (100 μg/mL) and incubated in the dark at 25°C for 3–4 days. Actively growing hyphal tips were transferred to potato dextrose agar (BD Difco, Sparks, MD, USA) and incubated under the same conditions for an additional 4 days. For pure culture isolation, single spores were isolated from sporulating colonies (Jang et al., 2024). For non-sporulating isolates, single hyphal tips were excised to establish monohyphal cultures. Pure cultures were preserved long-term by mixing conidia or hyphae with 15% glycerol in 2 mL sterile cryovials (Cryo.s 2 mL, Greiner Bio-One, Kremsmünster, Austria), allowing them to equilibrate at room temperature for 3 days before storage at –80°C.

***B. oryzae* species identification.** For molecular identification, genomic DNA was extracted from 7-day-old fungal cultures grown in 20 mL of potato dextrose (PD) broth (BD Difco) at 25°C and 120 rpm. Mycelia were harvested, lyophilized, and ground to a fine powder. DNA was extracted using the NucleoSpin Plant II kit (Macherey-Nagel, Düren, Germany) following the manufacturer's instructions. DNA concentration and purity were measured using a NanoDrop ND-1000 spectrophotometer (NanoDrop Technologies, Wilmington, DE, USA), and working stocks were adjusted to 12.5 ng/μL and stored at –20°C.

The internal transcribed spacer (ITS) region of rDNA was amplified by polymerase chain reaction (PCR) using the primer pair ITS1F (5′-TCCGTAGGTGAACCTGC-

GG-3′) and ITS4 (5′-TCCTCCGCTTATTGATATGC-3′) as described by Gardes and Bruns (1993) and White et al. (1990). PCR reactions were carried out in 20 µL volumes containing 25 ng of genomic DNA, 1 µL each of ITS1F and ITS4 primers (10 pmol/µL), 10 µL of 2× PCR Master Mix Solution (i-MAXII, iNtRON Biotechnology, Seongnam, Korea), and nuclease-free water. The PCR conditions were: initial denaturation at 94°C for 5 min; 30 cycles of 94°C for 30 s, 52°C for 1 min, and 72°C for 1 min; followed by a final extension at 72°C for 5 min. Amplified products were visualized by electrophoresis on a 0.8% agarose gel at 100 V for 30 min and observed under UV light. PCR products were sequenced by Macrogen (Daejeon, Korea). Raw sequences were assembled and edited using SeqMan (DNAStar Lasergene v7.1, DNASTAR, Madison, WI, USA), and species identity was confirmed by BLAST searches against the NCBI nucleotide database, with ≥99.5% sequence identity used as the identification threshold.

Whole genome sequencing. For whole genome sequencing, each isolate was cultured in 200 mL of PD broth at 25°C and 120 rpm for 7 days. On days 1 and 3 of culture, the mycelial mass was homogenized using a homogenizer (IKA Works Asia, Malaysia) to promote uniform growth. The fungal biomass was harvested by filtration through a single layer of Miracloth (Calbiochem, San Diego, CA, USA) and washed with 1 L of sterile distilled water to remove excess polysaccharides. Mycelia were dried on sterile paper towels and frozen at –20°C for 12 h or at -80°C for 1 h prior to lyophilization. Lyophilized material was ground to a fine powder using a pre-chilled mortar and pestle with liquid nitrogen.

Genomic DNA was extracted using the DNeasy Plant Mini Kit (Qiagen, Valencia, CA, USA) following the manufacturer's protocol. DNA quantity and concentration were assessed using a NanoDrop ND-1000 spectrophotometer (NanoDrop Technologies). Samples were sent to Macrogen for quality control assessment and whole genome sequencing. Sequencing was performed using both the Illumina NovaSeq platform for short paired-end reads and the PacBio Revio platform for long-reads. All data related to the genomes have been submitted to public repositories (Supplementary Data 1).

Genome assembly and structural annotation. The raw Illumina and PacBio reads were preprocessed using default option Fastp v0.24.0 and Fastplong v0.2.2, respectively (Chen, 2023). The filtered long-read data were assembled into contigs using Flye v2.9.5 with a genome size estimate of 34 Mb (Kolmogorov et al., 2019). To improve the accuracy of the assembled contigs, error correction was performed using default option Pilon v1.24 with the corresponding short-read mapping data generated by BWA-MEM v2.2.1 (Li, 2013; Walker et al., 2014). Subsequently, scaffolding of contigs was performed using RagTag v2.1.0, with the Nanopore-assembled genome of strain Bo-1 serving as the reference (Alonge et al., 2022; Liu et al., 2024). Mitochondrial sequences were removed from the assembled genomes by BLAST mapping against the previously published mitochondrial genome of *B. oryzae* (Deng et al., 2019). Genome assembly quality was assessed using BUSCO v5.8.2 with the fungi_odb12 and ascomycota_odb12 lineage datasets (Manni et al., 2021).

To enable comprehensive comparative genomic analysis, *de novo* repeat identification was performed on the newly assembled *B. oryzae* genomes as well as other genomes used in this study, using RepeatModeler v2.0.5 with LTRStruct and slow search options and RepeatMasker v4.1.8 (Chen, 2004; Flynn et al., 2020). Gene structure annotation was subsequently conducted using BRAKER3 with fungus option, which integrates fungal *ab initio* gene prediction with protein homology evidence (Gabriel et al., 2024). For protein evidence, a total of 1,471,133 protein sequences belonging to the Pleosporaceae family were retrieved from the NCBI non-redundant (NR) database and used to guide annotation.

Functional annotation and gene family prediction. The functions of genes predicted through structural annotation were analyzed based on their protein sequences using OmicsBox v3.5.4 with NR, gene ontology (GO) term, and InterPro searches (BioBam Bioinformatics, 2019). GO term enrichment analysis for lineage-specific genes in *Bipolaris* species was performed using Fisher's Exact Test implemented in OmicsBox, with a significance threshold of P-value < 0.05. Carbohydrate-active enzymes (CAZymes) were predicted using default option dbCAN v4.1.4 (Zheng et al., 2023), while proteases and lipases were identified through BLASTp searches against the MEROPS database (release 12.4) and the Lipase Engineering Database (LED v4.1.0), respectively (Fischer and Pleiss, 2003; Rawlings et al., 2010). Putative effectors and secreted proteins were predicted using the fungal mode EffectorP v3.0 and the fast and eukaryote mode of SignalP v6.0, respectively (Sperschneider and Dodds, 2022; Teufel et al., 2022). Finally, SMBGCs were identified using relaxed mode of antiSMASH v7.1.0 with all options on (Blin et al., 2023).

Genomic synteny, single nucleotide polymorphisms, and phylogenomic analyses. Synteny between species and strains was analyzed using the nucmer tool from the MUMmer v4.0.0rc1 package, and single nucleotide polymorphisms (SNPs) were identified from the aligned genomes using dandiff (Marçais et al., 2018). For phylogenomic analysis, to determine the phylogenetic position of *B. oryzae* strains isolated from South Korea within the Pleosporaceae family, genome assembly sets of representative species from the genera *Bipolaris*, *Pyrenophora*, *Alternaria*, *Stemphylium*, and *Exserohilum* were downloaded from NCBI (Supplementary Table 1, https://doi.org/10.6084/m9.figshare.28979261). Ortholog clustering was performed based on predicted protein sequences using OrthoFinder v2.5.4 (Emms and Kelly, 2019). Multiple sequence alignment of orthologs was carried out with MAFFT v7.490, gene trees were inferred using FastTree v2.1.11, and the species tree was reconstructed with IQ-TREE v3.0.1 using automatic model detection and 1,000 bootstrap replicates under the maximum likelihood framework (Katoh and Standley, 2013; Price et al., 2010; Wong et al., 2025).

Results

Genomic characteristics of *B. oryzae* strains. The genomes of newly sequenced *B. oryzae* isolates, assembled using long-read sequencing data, comprised 18 to 38 scaffolds and ranged in size from 34.26 to 36.08 Mbp. These sizes are comparable to that of the reference strain Bo-1, which consists of 18 scaffolds totaling 35.82 Mbp (Table 1). Among species with high-quality genome assemblies, the genome size of *B. oryzae* was similar to that of *B. zeicola* (isolate GZL10) (Xia et al., 2022), but approximately 1 Mbp smaller than those of *B. maydis* and *B. sorokiniana* strains (Fig. 1A, Supplementary Table 1). These estimates exclude mitochon-

Table 1. The genome statistics of *Bipolaris oryzae* strains

Strain	F1248	F1253	F1305	F1318	F1371	F1409	Bo-1	TG12bL2	ATCC 44560 (WK-1C)
Origin	Korea	Korea	Korea	Korea	Korea	Korea	China	USA	China (Taiwan)
Host	*Oryza sativa* (leaf)	*O. sativa* (leaf)	*O. sativa* (grain)	*O. sativa* (neck)	*O. sativa* (leaf)	*O. sativa* (leaf)	*O. sativa* (leaf)	*Z. palustris* (leaf)	*O. sativa* (leaf)
Mating type	1-1	1-2	1-1	1-1	1-2	1-1	Unknown	Unknown	1-2
Seq. Tech.	PacBio, Illumina	PacBio, Illumina	PacBio, Illumina	PacBio, Illumina	PacBio, Illumina	PacBio, Illumina	ONT, MGI	Illumina	Illumina
Long-read coverage (×)	26.2	25.0	22.8	19.2	46.1	38.8	-	-	-
Genome size (bp)	34,258,768	34,553,023	35,772,609	36,076,242	34,278,417	34,611,244	35,820,980	31,579,737	31,246,909
# scaffolds	19	18	35	38	21	20	18	1,623	594
N50	2,204,177	2,259,043	2,399,092	2,288,353	2,161,298	2,176,756	2,397,707	75,123	135,538
L50	6	6	6	6	6	6	6	130	67
GC (%)	48.82	49.86	49.87	49.85	49.89	49.62	49.97	50.98	50.58
BUSCO (%)	98.7	98.7	98.8	98.8	98.7	98.8	98.8	98.8	98.8
Repeat (bp)	3,819,210	3,990,870	5,304,173	5,571,583	4,047,054	4,114,679	5,139,101	1,112,615	989,503
WGS accession	JBMDHX01	JBMDHY01	JBMDHZ01	JBMDIA01	JBNFYF01	JBNFYG01	JAYECM01	LNFW01	AMCO01
No. of mitogenomes	1	1	1	1	1	1	1	17	25
Mitogenome size (bp)	129,186	129,490	130,943	130,943	128,094	128,112	172,104	95,793	116,988
Reference	This study	This study	This study	This study	This study	This study	Liu et al. (2024)	Castell-Miller et al. (2016)	Condon et al. (2013)

WGS, whole genome sequencing.

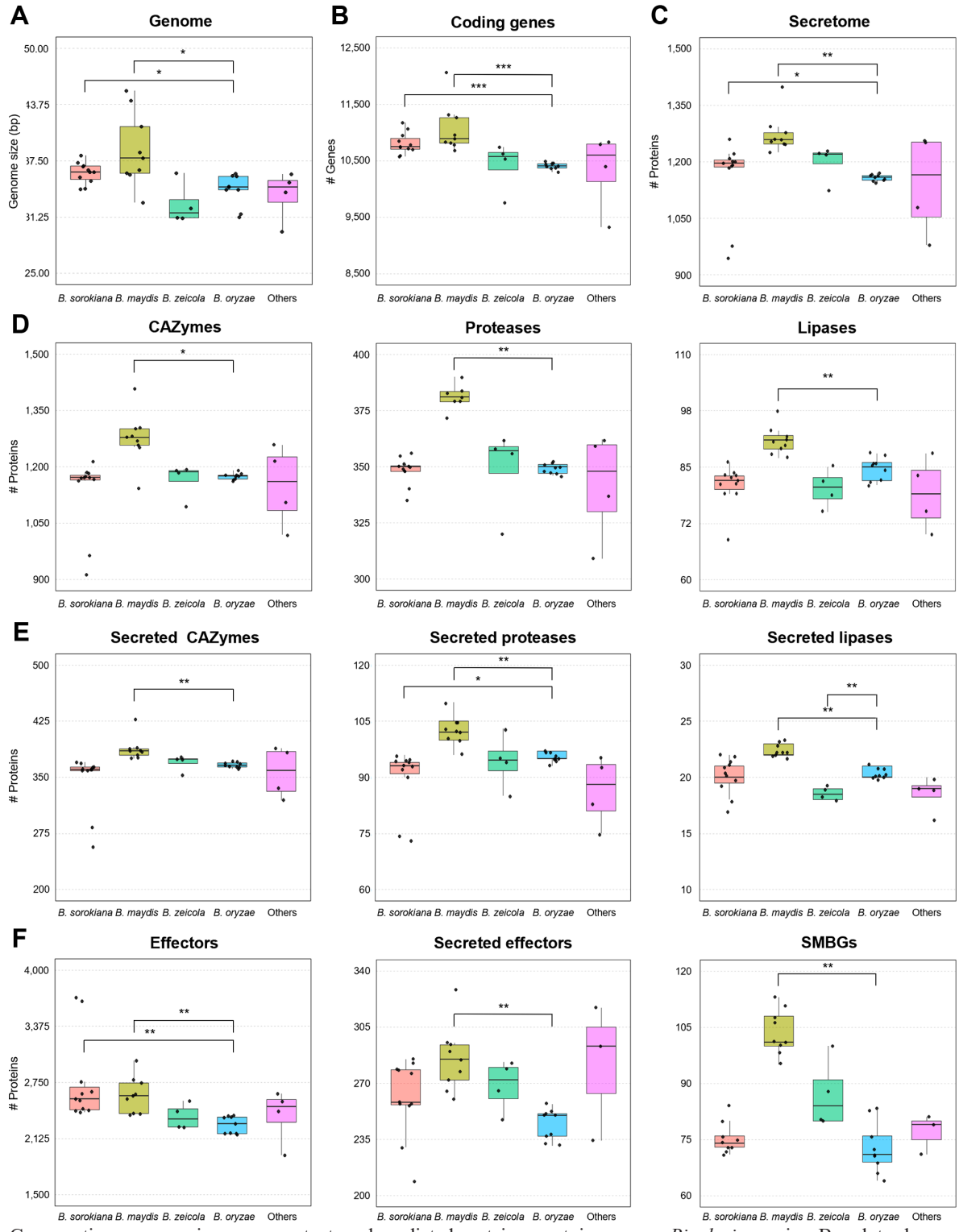

Fig. 1. Comparative genome size, gene content, and predicted protein repertoires across *Bipolaris* species. Boxplots show variation in genome size (A), number of protein-coding genes (B), secreted proteins (C), and key functional categories including CAZymes, proteases, and lipases (D), and their secreted counterparts (E). (F) Variation in both total and secreted effectors, as well as secondary metabolite biosynthesis genes (SMBGs), is also presented across *Bipolaris* species. Species groups are color-coded, and pairwise Wilcoxon rank sum exact test was performed between *B. oryzae* and the other groups. Only statistically significant differences are indicated with asterisks. Asterisks denote significance levels as follows: *$P < 0.05$, **$P < 0.01$, ***$P < 0.001$. Individual dots represent the values for each genome within the respective group.

drial genome, for which an average size of 129 kbp was predicted across all *B. oryzae* isolates. The GC content of the long-read assemblies ranged from 48.82% to 49.97%, which is 0.5–1% lower than that of the short-read-based assemblies. Notably, long-read assemblies were 3–5 Mbp larger than the short-read assembled isolates, a difference largely attributable to improved resolution of repetitive regions (Table 1). This observation supports the enhanced capacity of long-read sequencing to span and assemble repetitive elements. Assessment of genome completeness using BUSCO further confirmed the high quality of the assemblies, with the majority of conserved fungal genes recovered in each isolate (Supplementary Fig. 1).

Comparison of gene family content between *B. oryzae* and other *Bipolaris* species. The number of gene families identified in each strain analyzed in this study is summarized in Supplementary Table 2. In addition to differences in genome size, *B. oryzae* also showed a significantly lower number of protein-coding genes compared to *B. sorokiniana* and *B. maydis* (Fig. 1B). Among *B. oryzae* strains, the number of annotated genes ranged from 10,298 (F1371) to 10,490 (F1253), whereas most strains of *B. victoriae*, *B. bicolor*, *B. zeicola*, *B. maydis*, and *B. sorokiniana* had over 10,500 predicted genes (Table 2). The predicted secretome of *B. oryzae* ranged from 1,144 (Bo-1) to 1,170 (F1409) proteins, which was significantly smaller than that of *B. sorokiniana* and *B. maydis* (Fig. 1C). Regarding nutrient-related enzymes, including CAZymes, proteases, and lipases, *B. maydis* possessed the highest number of genes among *Bipolaris* species and showed significant differences from *B. oryzae* (Fig. 1D). A similar pattern was observed for secreted forms of these enzymes, with *B. maydis* having the largest repertoire. However, *B. oryzae* was found to have more secreted proteases than *B. sorokiniana*, and more secreted lipases than *B. zeicola* (Fig. 1E). Additionally, *B. oryzae* had fewer predicted effectors, secreted effectors, and SMBGCs compared to other *Bipolaris* species, with statistically significant differences primarily observed in comparison with *B. maydis* (Fig. 1F). These results suggest that *B. oryzae* may have undergone a moderate contraction in gene families related to pathogenicity and nutrient acquisition, which could reflect species-specific adaptations in its ecological or host interaction strategies.

Phylogenomic relationships of species in the family Pleosporaceae. A phylogenomic tree was constructed based on 1,367 single-copy orthologs shared among 64 representative species within the Pleosporaceae family. Using *Exserohilum turcica* as the outgroup, the tree resolved major genera including *Bipolaris*, *Pyrenophora*, and *Alternaria* as distinct monophyletic lineages (Fig. 2A). Due to the use of an outgroup, the phylogenetic relationships among intraspecific strains, which exhibit relatively low genetic variation, are more clearly presented in Supplementary Fig. 2. Within the *Bipolaris* clade, *B. cookei* served as the basal outgroup, supporting the monophyly of the remaining *Bipolaris* species. Among them, *B. sorokiniana* and *B. maydis* formed a closely related pair, while *B. zeicola*, *B. victoriae*, and *B. bicolor* grouped together in a single clade. This clade was sister to *B. oryzae*, which formed a separate monophyletic lineage with *B. gigantea* placed as its outgroup. In addition, phylogenomic analysis clarified the taxonomic identity of the endophytic *Bipolaris* sp. L1-

Table 2. Number of CAZymes, proteases, lipases, effectors, and core SMBGs in *Bipolaris oryzae* strains

Strain	F1248	F1253	F1305	F1318	F1371	F1409	Bo-1	TG12bL2	ATCC 44560 (WK-1C)
Protein-coding genes	10,364	10,490	10,399	10,459	10,298	10,451	10,441	10,407	10,374
Proteins	11,882	11,980	11,882	11,941	11,773	11,951	11,852	11,901	11,852
CAZymes	1,181	1,167	1,178	1,175	1,161	1,177	1,174	1,190	1,165
Secreted CAZymes	364	369	366	371	364	368	361	371	363
Proteases	351	352	350	346	348	347	352	350	347
Secreted protease	96	93	97	97	95	94	97	95	95
Lipases	85	82	81	86	88	84	88	86	82
Secreted lipases	21	20	20	20	20	21	20	21	20
Effectors	2,363	2,188	2,360	2,167	2,289	2,182	2,376	2,181	2,380
Secreted effectors	257	232	250	231	251	237	250	238	252
SMBGs	217	214	226	229	210	218	240	183	188

CAZyme, carbohydrate-active enzymes; SMBGs, secondary metabolite biosynthesis genes (core + additional gene identified by antiSMASH).

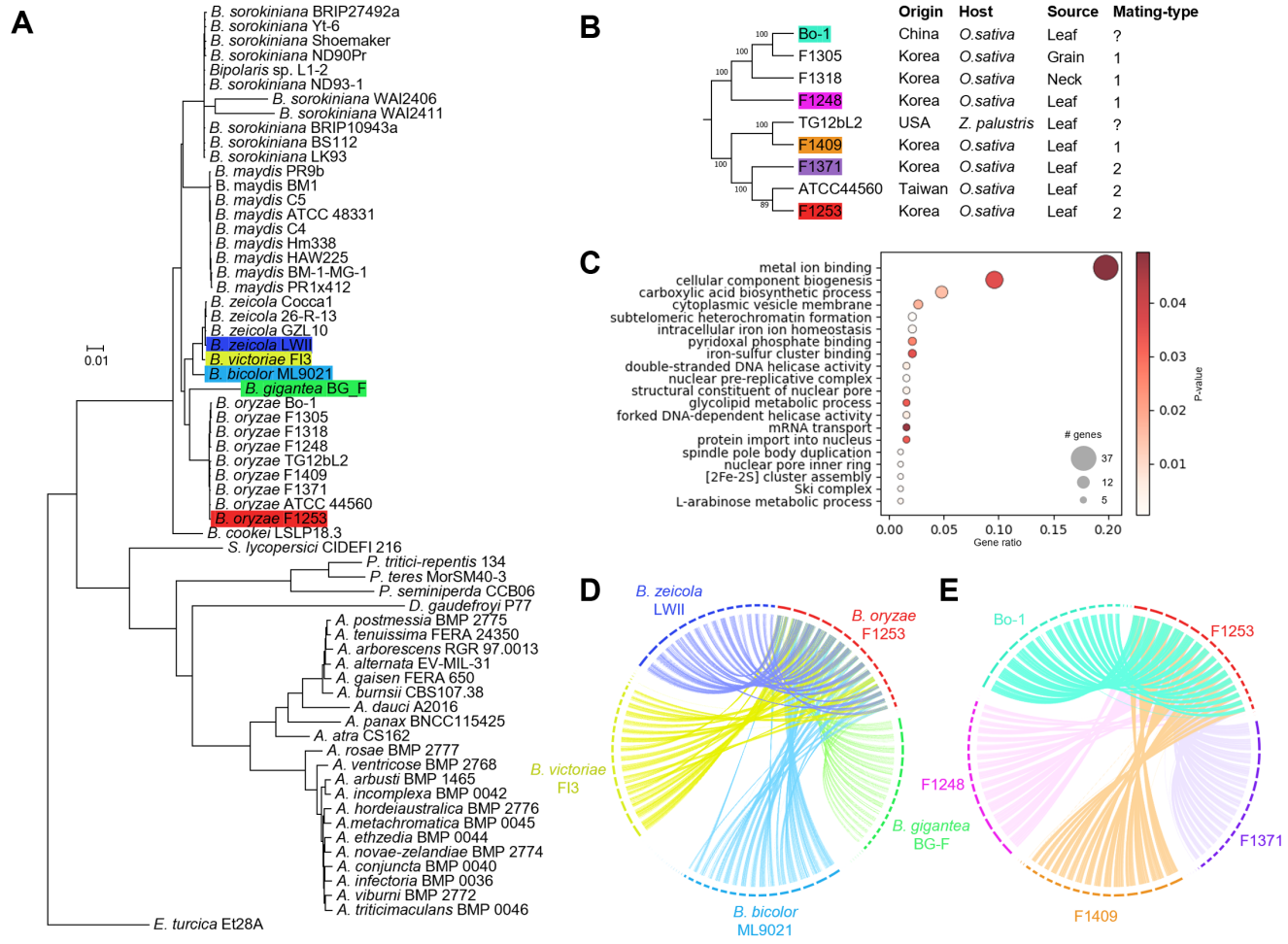

Fig. 2. Phylogenomic relationships and synteny analysis of *Bipolaris oryzae* and related species in the Pleosporaceae family. (A) Maximum-likelihood phylogenomic tree constructed using 1,367 single-copy orthologs from 64 strains across the Pleosporaceae family. (B) Subtree of *B. oryzae* strains showing their phylogenetic relationships, along with associated metadata including geographic origin, host, isolation source, and mating type. Bootstrap support values are indicated on each branch. (C) Gene ontology (GO) enrichment analysis of genes differentiating the two major clades within *B. oryzae*, highlighting biological processes associated with clade-specific orthogroups. Bubble size reflects the number of genes per GO term and color indicates significance level (*P*-value). (D) Circos plot showing synteny between *B. oryzae* F1253 and five other *Bipolaris* species: *B. gigantea* BG-F, *B. bicolor* ML9021, *B. victoriae* FI3, *B. zeicola* LWII, and *B. maydis* BM1. (E) Circos plot showing synteny between *B. oryzae* F1253 and four other *B. oryzae* isolates (F1248, F1371, F1409, Bo-1). Strains in panels (D) and (E) are color-coded and correspond to the highlights in (A) and (B).

2, confirming that it is a strain of *B. sorokiniana* (Long et al., 2019).

Within the *B. oryzae* lineage, two distinct clades were observed (Fig. 2B). However, no grouping patterns were associated with geographic origin, host species, infected tissue, or mating type (Supplementary Fig. 3). The Chinese strain Bo-1, isolated from rice, clustered with Korean strains that infect rice grain, neck, and leaf. The U.S. strain TG12bL2, isolated from *Zizania palustris*, grouped with the Korean strain F1409, which infects rice leaves. Additionally, Korean strains F1371 and F1253, both isolated from rice leaves, clustered with the Taiwanese strain ATCC 44560. This suggests that the phylogenetic relationships among strains are not clearly correlated with host or regional origin. This clade separation was primarily driven by sequence variation in 187 out of 1,367 single-copy orthologs. Functional enrichment analysis revealed that these divergent orthologs were significantly associated with processes such as metal ion binding, intracellular iron ion homeostasis, carboxylic acid biosynthetic process, DNA helicase activity, mRNA transport, and nuclear pore complex assembly (Fig. 2C). These results suggest that differentiation between *B. ory-*

zae clades may be linked to variation in genes involved in metabolism, genome maintenance, and cellular transport mechanisms.

Genomic synteny between *Bipolaris* species and *B. oryzae* strains. Synteny analysis using *B. oryzae* strain F1253 as a reference revealed that more extensive alignments were observed with phylogenetically closer *Bipolaris* species, although the quality of genome assemblies may influence alignment extent (Fig. 2D). For example, *B. gigantea* and *B. bicolor*, both assembled using short-read data, showed relatively high levels of genome alignment. Approximately 65% of the genome aligned with *B. zeicola*, the most distantly related species within the same clade, and with *B. sorokiniana*, which belongs to a different clade. In comparison, *B. maydis* showed approximately 60% genome alignment (Table 3). At the SNP level, *B. gigantea*, the sister species of *B. oryzae*, exhibited the lowest SNP count against F1253, with 1,630,671 SNPs. Other *Bipolaris* species showed similarly high SNP numbers ranging from 1.63 to 1.83 million, regardless of their phylogenetic positions. These results indicate substantial nucleotide-level divergence even among relatively closely related *Bipolaris* species.

In contrast, synteny among *B. oryzae* isolates showed a clearer correlation with phylogenetic clustering. Isolates within the same clade as F1253 exhibited high syntenic similarity, ranging from 91.0% to 98.8%. Isolates from the sister clade showed relatively lower synteny levels, ranging from 84.2% to 89.4% (Table 4, Fig. 2E). SNP comparisons supported these observations, with the number of SNPs decreasing markedly in isolates phylogenetically closer to F1253. For example, ATCC 44560, the most closely related isolate within the same clade, differed by only 12,793 SNPs. In contrast, F1409, another rice isolate, showed 69,519 SNPs, which was higher than that observed for TG-12bL2, a strain isolated from *Z. palustris*. Isolates from the sister clade had between 96,421 and 109,873 SNPs when compared to F1253 (Table 4). These findings demonstrate strong genomic coherence within clades of *B. oryzae*, while also revealing considerable variation between clades and even among strains isolated from the same host plant.

Ortholog diversity and functional signatures of *Bipolaris* and *B. oryzae* genomes. Ortholog clustering of predicted proteins from members of the Pleosporaceae

Table 3. Number of SNPs between *Bipolaris oryzae* F1253 and other *Bipolaris* species

Name	Total bases	Aligned bases	Aligned bases (%)	Total SNPs	SNP proportion (%)
Bipolaris cookei LSLP18.3	36,006,766	21,245,485	59.00	1,770,025	4.92
Bipolaris maydis BM1	36,126,374	21,796,041	60.33	1,782,232	4.93
Bipolaris sorokiniana LK93	36,231,650	23,612,716	65.17	1,830,975	5.05
Bipolaris zeicola LWII	32,215,838	21,157,436	65.67	1,637,131	5.08
Bipolaris victoriae FI3	33,973,299	23,288,879	68.55	1,808,781	5.32
Bipolaris bicolor ML9021	34,208,973	23,340,267	68.23	1,813,489	5.30
Bipolaris gigantea BG_F	28,449,892	19,109,920	67.17	1,630,671	5.73

SNP, single nucleotide polymorphism.

Table 4. Number of SNPs between *Bipolaris oryzae* F1253 and other *B. oryzae* strains

Name	Total bases	Aligned bases	Aligned bases (%)	Total SNPs	SNP proportion (%)
F1248	34,258,768	30,638,000	89.43	109,873	0.32
Bo-1	35,820,980	30,247,988	84.44	96,421	0.27
F1305	35,772,609	30,326,578	84.78	98,606	0.28
F1318	36,076,242	30,382,826	84.22	98,891	0.27
TG12bL2	31,652,537	30,155,676	95.27	40,623	0.13
F1409	34,611,244	31,481,847	90.96	69,519	0.20
F1371	34,278,417	32,770,267	95.60	25,151	0.07
ATCC 44560	31,289,209	30,903,173	98.77	12,793	0.04

SNP, single nucleotide polymorphism.

family resulted in a total of 24,924 orthogroups. Among these, 15,514 orthogroups included at least one *Bipolaris* species, representing the *Bipolaris* pan-genome, and 4,116 orthogroups were identified as *Bipolaris*-specific (Fig. 3A). Approximately 75% of the *Bipolaris*-specific orthogroups (3,082) were species-specific. *B. sorokiniana*, which had the highest number of predicted coding genes among the species analyzed, also contained the greatest number of species-specific orthogroups, totaling 1,548 (Fig. 3B). In contrast, *B. zeicola* and *B. oryzae*, despite having similar numbers of coding genes, had considerably fewer species-specific orthogroups, with 168 and 325 respectively. Among the *Bipolaris*-specific orthogroups, 36 were conserved across all 37 *Bipolaris* isolates analyzed and were defined as *Bipolaris*-specific core orthogroups. Additionally, 45, 154, 24, and 44 species-specific core orthogroups were identified in *B. sorokiniana*, *B. maydis*, *B. zeicola*, and *B. oryzae* respectively, indicating genes consistently

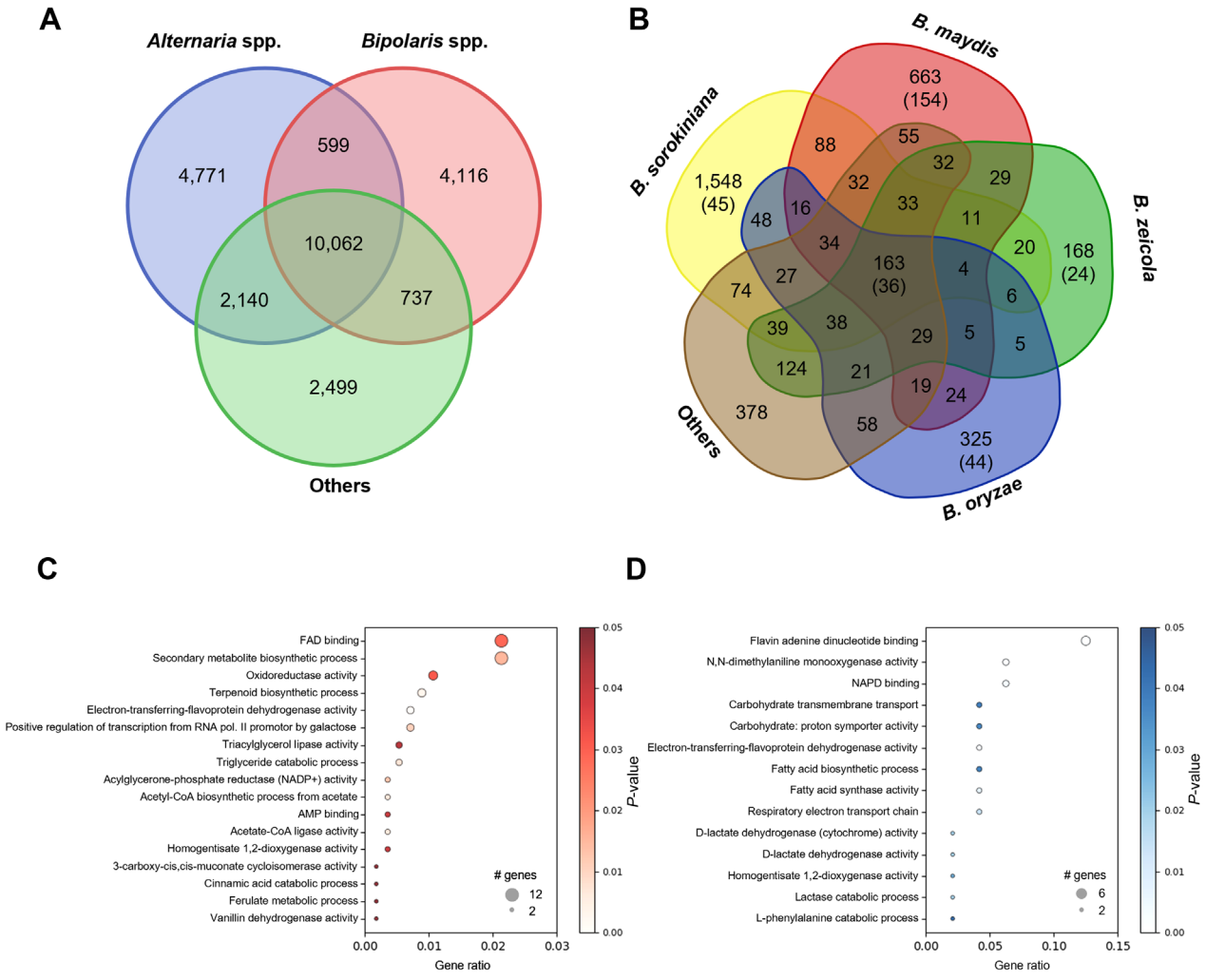

Fig. 3. Orthologous group distribution and functional enrichment of *Bipolaris*-specific and *B. oryzae*-specific genes. (A) Venn diagram showing the total orthogroup distribution across all analyzed *Pleosporaceae* species. Red, blue, and green circles represent orthogroups specific to *Bipolaris*, *Alternaria*, and other genera, respectively. (B) Venn diagram illustrating the number of species-specific and shared orthogroups among the *Bipolaris* species (*B. sorokiniana*, *B. maydis*, *B. zeicola*, *B. oryzae,* and other *Bipolaris* spp.). Numbers in parentheses indicate the number of species-specific core orthogroups, which are conserved across all isolates within each species. (C) Gene ontology (GO) enrichment of *Bipolaris*-specific orthogroups (4,116) showing significant overrepresentation in functions related to FAD binding, secondary metabolite biosynthesis, oxidoreductase activity, terpenoid metabolism, and lipid degradation. (D) GO enrichment of *B. oryzae*-specific core orthogroups (44) showing enrichment in oxidoreductase activity, electron transport, carbohydrate transport, and the catabolism of fatty acids, lactate, and aromatic amino acids. Bubble sizes reflect the number of annotated genes, and color intensity indicates the statistical significance (*P*-value).

retained within each species. Strain-specific orthogroups varied among clades. In *B. oryzae*, the number ranged from 10 in strain F1305 to 25 in strain F1238, with an average of 17 per strain (Supplementary Fig. 4).

Functional enrichment analysis revealed that *Bipolaris*-specific orthogroups are enriched in functions related to metabolic specialization, including FAD binding, secondary metabolite biosynthesis, oxidoreductase activity, and lipid degradation (Fig. 3C). These features likely contribute to the genus's necrotrophic lifestyle by facilitating the breakdown of host-derived compounds and the production of bioactive metabolites involved in pathogenicity or environmental adaptation. Within this lineage, the 36 core orthogroups conserved across *B. oryzae* isolates were associated with carbohydrate and amino acid metabolism, including sucrose and maltose catabolism, amylase and glucosidase activity, and threonine degradation, highlighting shared mechanisms for utilizing plant-derived nutrients (Supplementary Figs. 5 and 6). In addition, 44 *B. oryzae*-specific core orthogroups showed enrichment in oxidoreductase functions, electron transport chain components, monooxygenase activity, and the catabolism of fatty acids, lactate, and aromatic amino acids (Fig. 3D). These species-specific functions may reflect evolutionary adaptations in energy metabolism and detoxification pathways, potentially contributing to the efficient utilization of host substrates and ecological success of *B. oryzae*.

SMBGCs in *B. oryzae* and *Bipolaris* species. Prediction of SMBGCs in *B. oryzae* F1253 identified 48 clusters, of which 12 showed homology to known biosynthetic gene clusters in the MIBiG database (Fig. 4A) (Terlouw et al., 2023). Notably, clusters responsible for the production of alternapyrone, 1,3,6,8-tetrahydroxynaphthalene, choline, and dimethylcoprogen exhibited 100% sequence identity with their MIBiG counterparts. Alternapyrone

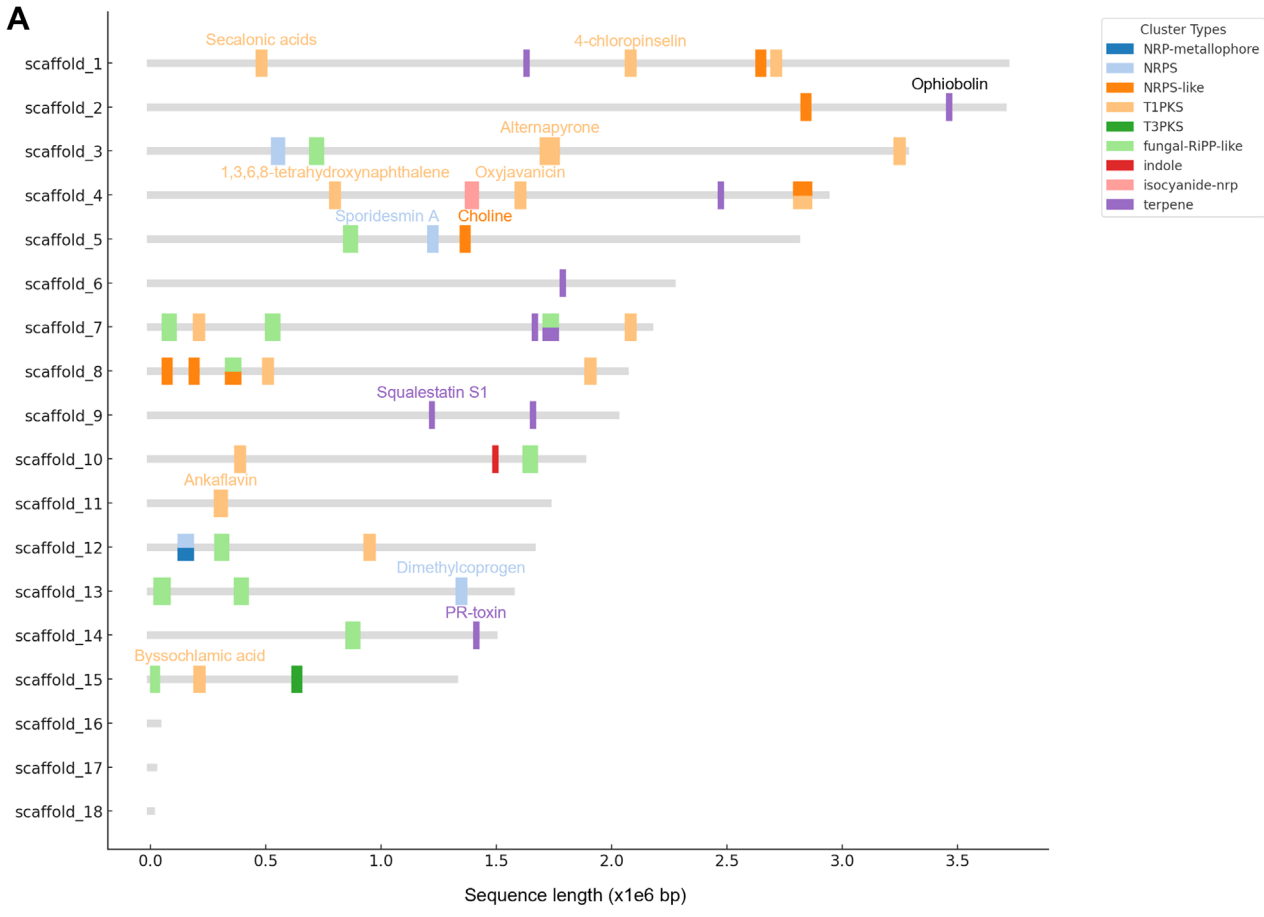

Fig. 4. Secondary metabolite biosynthetic gene clusters (SMBGCs) identified in *B. oryzae* F1253 and other *Bipolaris* species/strains. (A) Distribution of SMBGCs predicted from the genome of *B. oryzae* strain F1253. Each colored box represents a predicted SMBGC, classified by biosynthetic gene cluster type. Clusters homologous to known SMBGCs in the MIBiG database are labeled with their corresponding secondary metabolites. (Continued)

Fig. 4. (Continued) (B) Heatmap showing cluster similarity (%) of SMBGCs identified across multiple *Bipolaris* isolates compared with known SMBGCs in the MIBiG database. The intensity of red color indicates the level of sequence conservation, ranging from 0% (white) to 100% (dark red). The heatmap highlights differential conservation patterns across various secondary metabolites, suggesting lineage-specific evolution and metabolic adaptation within the genus.

is a polyketide mycotoxin known for phytotoxic effects; 1,3,6,8-tetrahydroxynaphthalene is a precursor of DHN-melanin, important for fungal protection and pathogenicity; choline functions as a phospholipid precursor and osmoprotectant; and dimethylcoprogen is a siderophore involved in iron acquisition. Additional SMBGCs showed partial similarity (9–70%) to clusters involved in the biosynthesis of secalonic acid (a toxic dimeric tetrahydroxanthone), 4-chloropinselin and related halogenated polyketides, oxyjavanicin (a fungal meroterpenoid), sporidesmin A (an epipolythiodioxopiperazine mycotoxin), squalestatin S1 (a squalene synthase inhibitor), ankaflavin (a benzoisochromanequinone derivative), PR-toxin (a known food-contaminating mycotoxin), and byssochlamic acid (a bioactive polyketide) (Fig. 4B). These results suggest that *B. oryzae* possesses the genetic potential to produce both known and structurally related novel secondary metabolites.

A broader analysis of SMBGCs across 37 *Bipolaris* isolates predicted a total of 48 known clusters (Fig. 4B). Among these, the melanin precursor 1,3,6,8-tetrahydroxynaphthalene and the choline biosynthetic cluster were fully conserved across all strains, indicating their essential roles in fungal survival and host interaction. In contrast, clusters encoding squalestatin S1 and secalonic acids were present at low conservation levels across the species, suggesting variability in toxin biosynthesis potential. The alternapyrone and dimethylcoprogen clusters showed a clade-specific pattern, being completely conserved in all species except *B. sorokiniana* and *B. zeicola*, respectively. Other SMBGCs, including those encoding halogenated polyketides (4-chloropinselin, pinselin, chloromonilinic acids, 4-hydroxyvertixanthone), tetramic acid derivatives (e.g., AbT1), PR-toxin, HEx-pks1-related polyketides, betaenones, ACT-toxin II, and acetylaranotin, were found only in specific species (*B. maydis* and *B. oryzae*) or in subsets of strains. This distribution suggests that while *Bi-*

polaris species maintain a conserved core set of secondary metabolism genes for essential functions, they have also undergone differential gain or loss of accessory metabolite clusters. Such variation likely reflects adaptive evolution in response to host specificity or ecological niches.

Conservation and evolution of ophiobolin biosynthetic gene clusters in *Bipolaris* species. Although *B. oryzae* is known to attack its hosts using the phytotoxin ophiobolin, the genomic location of its biosynthetic gene cluster had not previously been characterized in this species. Using sequence homology analysis based on the known ophiobolin biosynthetic cluster (*oblA*, *oblB*, *oblC*, and *oblD*) identified from *Aspergillus ustus* 094102, we located the corresponding cluster in *B. oryzae* strain F1253 at the distal region of pseudochromosome 2 (scaffold 2), where it exists as a predicted SMBGC (Fig. 4A). Additional homology searches across other *Bipolaris* species indicated that complete clusters containing *oblA* through *oblD* were present in *B. cookei*, *B. oryzae*, *B. maydis*, and *B. sorokiniana*. In contrast, clusters lacking *oblC* were observed in *B. bicolor*, *B. victoriae*, and *B. zeicola* (Fig. 5) (Chai et al., 2016; Yan et al., 2022). However, this does not imply the complete absence of oblC homologs. Instead, homologous sequences were identified outside the primary cluster. Further examination revealed substantial differences in intergenic distances within the ophiobolin biosynthetic clusters among *Bipolaris* species. Repeat analysis showed the presence of numerous simple repeats, with notably longer intergenic regions in *B. zeicola*, *B. sorokiniana*, and *B. cookei*. These regions contained insertions of repeat elements, including DNA transposons, long terminal repeat (LTR) retrotrans-

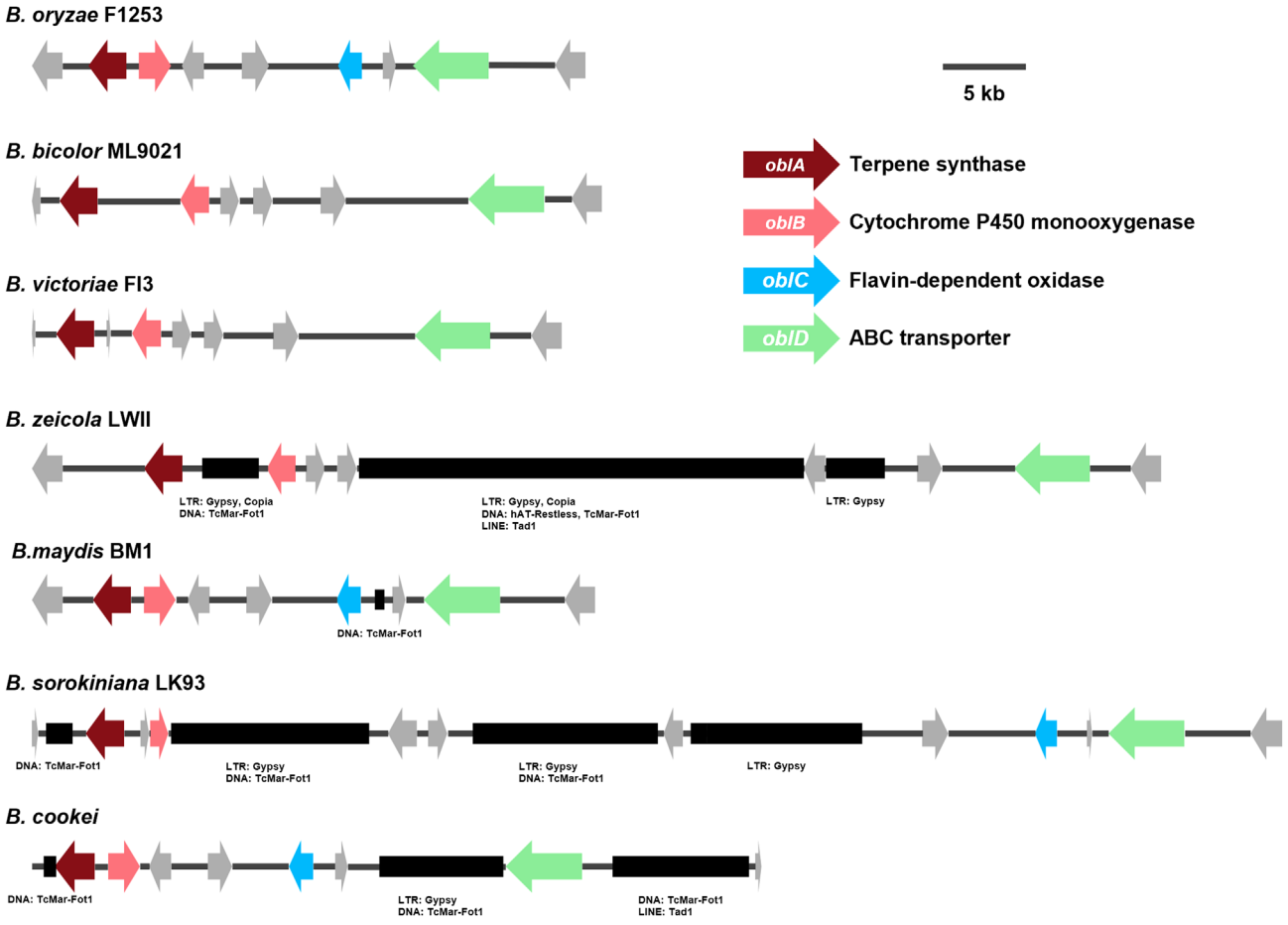

Fig. 5. Organization of the ophiobolin biosynthetic gene cluster in *Bipolaris* species. The schematic illustrates the genomic arrangement of four key ophiobolin biosynthetic genes (*oblA*, *oblB*, *oblC*, and *oblD*) across representative *Bipolaris* isolates. Each gene is shown as a colored arrow indicating its coding orientation. Flanking and intervening genes not assigned to the core biosynthetic pathway are represented in gray. Black bars denote repetitive elements located within or adjacent to the gene cluster regions. These repetitive sequences are composed of complex repeat structures, including both known and simple repeats, although only the known repeat classes are visualized. Repeat orientation is omitted for clarity.

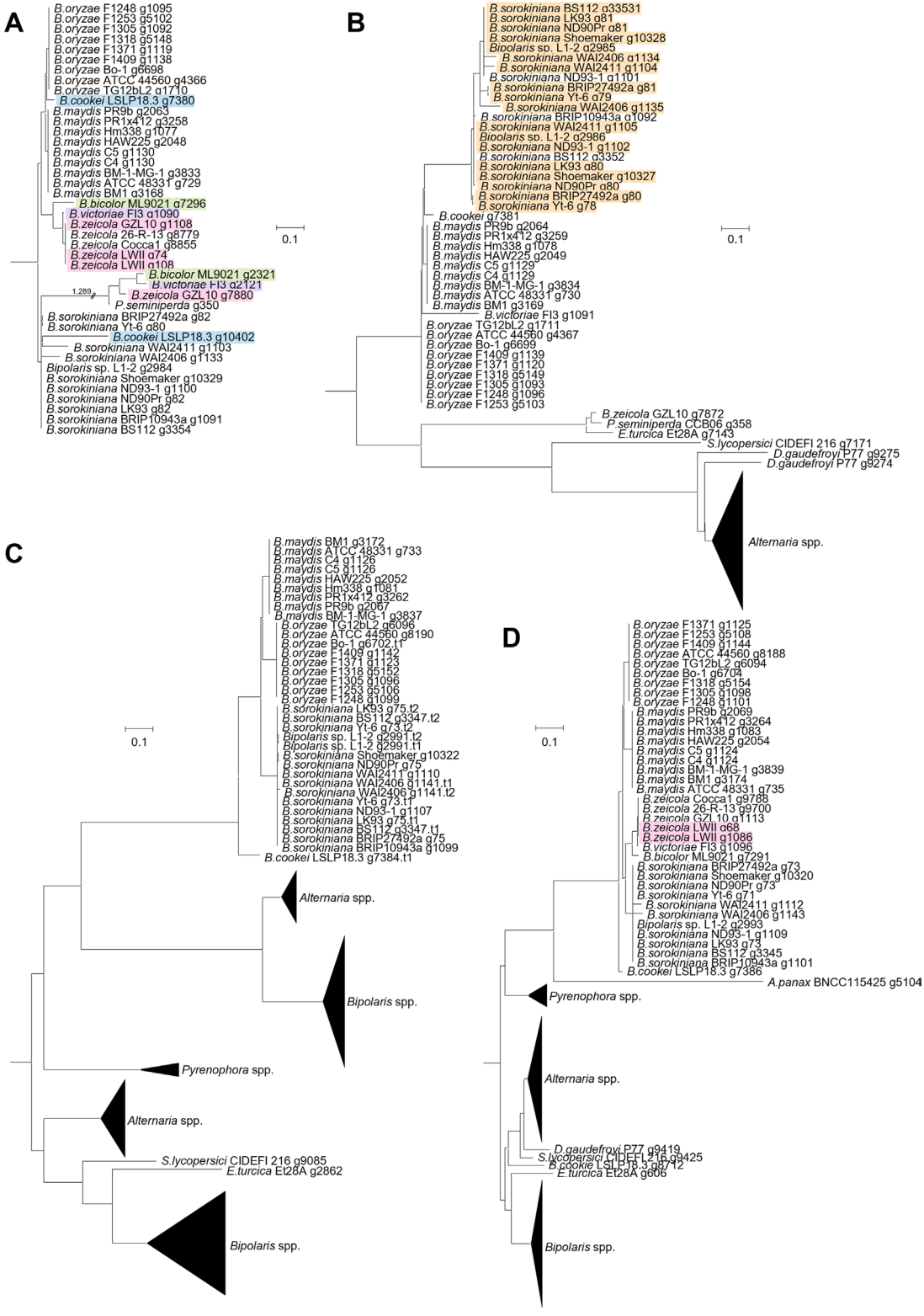

Fig. 6. Phylogenetic analysis of *obl* genes involved in ophiobolin biosynthesis in *Bipolaris* and related species. Maximum-likelihood phylogenetic trees of four ophiobolin biosynthetic genes were reconstructed using FastTree2. Each panel represents the gene tree of one gene: (A) *oblA*, (B) *oblB*, (C) *oblC*, and (D) *oblD*. Clades containing gene paralogs within a single strain are highlighted in color. Putative isoforms were only observed in oblC, where two transcript variants (t1, t2) were detected in *B. sorokiniana*, indicating possible alternative splicing or annotation of partial gene models.

posons, and long interspersed nuclear elements (LINEs).

Ortholog clustering across the broader Pleosporaceae family revealed unique distribution patterns among the *obl* genes. The *oblA* was exclusively detected in *Bipolaris* species and, notably, in *Pyrenophora seminiperda* (Fig. 6A). Single-copy orthologs of oblA were present in *B. oryzae*, *B. maydis*, and *B. sorokiniana*, whereas *B. bicolor*, *B. victoriae*, *B. cookei*, and *B. zeicola* contained additional paralogs. Conversely, *oblB*, *oblC*, and *oblD* were widely conserved across *Alternaria*, *Bipolaris*, and other *Pleosporaceae* species. Within *B. sorokiniana*, oblB was annotated as tandem paralogs due to mutations causing an internal stop codon (CCA to TGA) and an internal start codon, as evidenced by sequence alignment (Figs. 5 and 6B, Supplementary Fig. 7). The oblC orthologs grouped into three distinct clades within the genus *Bipolaris*, with an additional isoform detected specifically within the ophiobolin biosynthetic clade in *B. sorokiniana* (Fig. 6C). Finally, oblD formed two separate clades within *Bipolaris*, existing as a single-copy ortholog in all isolates within the ophiobolin biosynthetic clade, except for *B. zeicola* strain LWII (Fig. 6D). These observations suggest lineage-specific evolutionary trajectories and genomic plasticity of the ophiobolin biosynthetic gene clusters within *Bipolaris*, reflecting their adaptive significance in host interaction and ecological specialization.

Discussion

In this study, we collected genomic data from 37 strains representing eight species of *Bipolaris* within the Pleosporaceae family, performed genome re-annotation, and conducted comprehensive comparative analyses. The results elucidate the evolutionary dynamics, metabolic specialization, and secondary metabolite evolution in the necrotrophic plant pathogen *Bipolaris*, with a specific focus on *B. oryzae*.

The phylogenomic species/strain tree confirms that *Bipolaris* forms a well-supported monophyletic lineage within Pleosporaceae, clearly distinct from related genera such as *Pyrenophora* and *Alternaria* (Fig. 2A). This finding aligns with fungal systematics, which consistently demonstrates stable genus-level delineation within Pleosporales (Zhang et al., 2012). However, earlier phylogenies constructed using multi-loci approaches (ITS, GAPDH, TEF) and mitochondrial gene-based analyses have shown less consistent and sometimes conflicting relationships among *Bipolaris* species (Manamgoda et al., 2014; Song et al., 2024). Both ortholog-based and multi-loci-based species trees consistently placed *B. cookei* as the outermost (basal) group, yet they differed notably in the internal grouping of species within the genus. These discrepancies can be attributed primarily to limitations inherent in multi-loci phylogenies, such as insufficient phylogenetic signals, varying evolutionary rates among loci, incomplete lineage sorting, and potential biases introduced by gene selection. Moreover, mitochondrial phylogenies are particularly susceptible to genomic rearrangements and accelerated evolutionary rates, further complicating reliable species-level resolution. Therefore, genome-wide single-copy ortholog-based phylogenies, as conducted in this study, provide a more robust and reliable method for accurately resolving the evolutionary relationships within *Bipolaris*.

The genome sizes of *B. oryzae* (34–36 Mbp) closely resemble those of *B. zeicola*, yet are notably smaller (>1 Mbp difference) than those of *B. sorokiniana* and *B. maydis* (Fig. 1A). Our comparative genomic analysis further reveals that *B. oryzae* possesses fewer protein-coding genes and a reduced secretome repertoire compared to these two species (Fig. 1B and C). Similar genome contraction, especially involving candidate effectors, has been previously reported in *B. cookei* and may reflect evolutionary processes driven by niche specialization or host-specific adaptation within *Bipolaris* (Zaccaron and Bluhm, 2017). Notably, our findings indicate that *B. oryzae* exhibits a streamlined enzymatic toolkit tailored specifically to its necrotrophic lifestyle causing brown spot disease in rice; it contains fewer secreted CAZymes compared to *B. maydis*, but a higher number of secreted proteases relative to *B. sorokiniana* and an increased abundance of lipases compared to *B. zeicola* (Fig. 1D and E). In contrast, maize pathogens such as *B. maydis* demonstrate an expanded repertoire of CAZymes and SMBGCs, correlating with enhanced virulence and elevated expression during host infection (Meshram et al., 2022; Sheng et al., 2023). These genomic patterns suggest that *B. oryzae* may employ a refined, optimized arsenal uniquely adapted to rice as its primary host. Further comparative genomic analyses involving additional isolates of *B. oryzae* from diverse host plants beyond rice will be essential to confirm and expand upon these host-specific adaptive hypotheses.

Lastly, our study marks the first genomic confirmation of the ophiobolin biosynthetic cluster (oblA-D) at the telomeric region of pseudochromosome 2 in *B. oryzae*, mirroring the organization observed in *Aspergillus ustus* and other *Bipolaris* species (Figs. 4–6). While *B. cookei*, *B. oryzae*, *B. maydis*, and *B. sorokiniana* retain all four core genes, *B. bicolor*, *B. victoriae*, and *B. zeicola* show relocation of *oblC* outside the primary cluster, consistent with transposon-mediated cluster fragmentation (Zaccaron and Bluhm, 2017). The presence of repetitive elements such as DNA

transposons, LTRs, and LINEs within intergenic regions suggests ongoing genomic rearrangements that may facilitate gene cluster shuffling, a phenomenon widely observed among *Bipolaris* species (Condon et al., 2013). Phylogenetic analysis of individual *obl* genes further reveals paralogs and isoforms in certain *Bipolaris* species. For instance, *oblA* appears restricted to *Bipolaris* and the related grass pathogen *P. seminiperda*, suggesting a relatively recent lineage-specific acquisition (Fig. 6A) (Medd et al., 2003). In *B. sorokiniana*, *oblB* exists as tandem paralogs resulting from internal codon mutations, while *oblC* displays multiple isoforms and *oblD* is generally single-copy, except in *B. zeicola* LWII (Fig. 6B–D). These patterns highlight the evolutionary plasticity of SMBGCs in plant-pathogenic fungi, similar to transposon-associated expansions of toxin clusters seen in *Pyrenophora tritici-repentis* (Moolhuijzen et al., 2020). The conservation of ophiobolin biosynthesis genes in *B. oryzae*, alongside the expansion of degradative and metabolic pathways, supports a model in which this species employs a compact yet potent virulence toolkit that is effective in host colonization without the need for the extensive arsenal observed in more aggressive pathogens like *B. maydis*. Under climate-related stress conditions such as drought and elevated temperatures, weakened plant defenses may allow *B. oryzae* to exploit its existing metabolic capacity more efficiently, which aligns with recent observations of increased brown spot outbreaks in warm or water-limited rice-growing regions.

Our comparative genomics points to practical routes for mitigating brown spot under climate stress. The conserved ophiobolin cluster and its variable repeat context nominate *oblA* to *oblD* as surveillance markers. Quantitative PCR or amplicon sequencing, including copy number assays, can support regional risk assessment and seed testing in drought-prone systems (Edwards et al., 2001). Resistance breeding can adopt metabolite-informed screens using purified ophiobolin or producing isolates and select lines with smaller lesions and reduced leakage (Vidhyasekaran et al., 1986). Priority traits include membrane stability and glutathione-based detox capacity that can be assayed via electrolyte-leakage and redox markers (Zechmann, 2020). The ophiobolin cluster also offers sequence-defined targets for host- or spray-induced RNAi against the terpene cyclase and tailoring enzymes (Nunes and Dean, 2012). Given the repeat-rich, synteny-variable context of SMBGCs in *Bipolaris* and related fungi, integrate management by rotating chemistries, reducing drought and nutrient stress, and deploying resistant cultivars where diagnostics indicate high ophiobolin potential.

Overall, our comparative genomic analysis significantly expands current knowledge of *B. oryzae* biology, providing robust genomic evidence that can inform strategies for monitoring and managing brown spot disease. Future research should focus on functional validation of candidate genes identified in this study, particularly those involved in secondary metabolite biosynthesis and host interaction, to enhance understanding of pathogen virulence and to support the development of targeted disease control measures. In addition, time-resolved transcriptome analyses across key stages of plant infection, coupled with comprehensive metabolite profiling, will be essential to link gene-expression dynamics with metabolic outputs and to pinpoint stage-specific determinants of virulence.

Conflicts of Interest

No potential conflict of interest relevant to this article was reported.

Acknowledgments

This work was carried out with the support of "Cooperative Research Program for Agriculture Science & Technology Development (Project title: Research on assessing the impact of climate change on the increase in pests and diseases, and developing a system for evaluating resistance. Project No. RS-2024-00400211)" Rural Development Administration, Republic of Korea.

Electronic Supplementary Material

Supplementary materials are available at The Plant Pathology Journal website (http://www.ppjonline.org/).

References

Alonge, M., Lebeigle, L., Kirsche, M., Jenike, K., Ou, S., Aganezov, S., Wang, X., Lippman, Z. B., Schatz, M. C. and Soyk, S. 2022. Automated assembly scaffolding using RagTag elevates a new tomato system for high-throughput genome editing. *Genome Biol.* 23:258.

BioBam Bioinformatics. 2019. Omicsbox: bioinformatics made easy. BioBam Bioinformatics, Valencia, Spain.

Blin, K., Shaw, S., Augustijn, H. E., Reitz, Z. L., Biermann, F., Alanjary, M., Fetter, A., Terlouw, B. R., Metcalf, W. W., Helfrich, E. J. N., van Wezel, G. P., Medema, M. H. and Weber, T. 2023. antiSMASH 7.0: new and improved predictions for detection, regulation, chemical structures and visualisation. *Nucleic Acids Res.* 51:W46-W50.

Castell-Miller, C. V., Gutierrez-Gonzalez, J. J., Tu, Z. J., Bushley, K. E., Hainaut, M., Henrissat, B. and Samac, D. A. 2016.

Genome assembly of the fungus *Cochliobolus miyabeanus*, and transcriptome analysis during early stages of infection on American wildrice (*Zizania palustris* L.). *PLoS ONE* 11:e0154122.

Chai, H., Yin, R., Liu, Y., Meng, H., Zhou, X., Zhou, G., Bi, X., Yang, X., Zhu, T., Zhu, W., Deng, Z. and Hong, K. 2016. Sesterterpene ophiobolin biosynthesis involving multiple gene clusters in *Aspergillus ustus. Sci. Rep.* 6:27181.

Chen, N., 2004. Using RepeatMasker to identify repetitive elements in genomic sequences. *Curr. Protoc. Bioinformatics* Chapter 4:Unit 4.10.

Chen, S. 2023. Ultrafast one-pass FASTQ data preprocessing, quality control, and deduplication using fastp. *iMeta* 2:e107.

Condon, B. J., Leng, Y., Wu, D., Bushley, K. E., Ohm, R. A., Otillar, R., Martin, J., Schackwitz, W., Grimwood, J., MohdZainudin, N., Xue, C., Wang, R., Manning, V. A., Dhillon, B., Tu, Z. J., Steffenson, B. J., Salamov, A., Sun, H., Lowry, S., LaButti, K., Han, J., Copeland, A., Lindquist, E., Barry, K., Schmutz, J., Baker, S. E., Ciuffetti, L. M., Grigoriev, I. V., Zhong, S. and Turgeon, B. G. 2013. Comparative genome structure, secondary metabolite, and effector coding capacity across *Cochliobolus* pathogens. *PLoS Genet.* 9:e1003233.

Das, D., Chowdhury, N., Sharma, M., Suma, R., Saikia, B., Velmurugan, N. and Chikkaputtaiah, C. 2024. Screening for brown-spot disease and drought stress response and identification of dual-stress responsive genes in rice cultivars of Northeast India. *Physiol. Mol. Biol. Plants* 30:647-663.

Dasgupta, M. K. 1984. The Bengal famine, 1943 and the brown spot of rice: an inquiry into their relations. *Hist. Agric.* 2:1-18.

Deng, G., Zou, Q., Chen, Y., Wang, L., Huang, G., Cui, Y., Ding, M. and Wang, Y. 2019. The complete mitochondrial genome of *Cochliobolus miyabeanus* (Dothideomycetes, Pleosporaceae) causing brown spot disease of rice. *Mitochondrial DNA B Resour* 4:2832-2833.

Edwards, S. G., Pirgozliev, S. R., Hare, M. C. and Jenkinson, P. 2001. Quantification of trichothecene-producing *Fusarium* species in harvested grain by competitive PCR to determine efficacies of fungicides against Fusarium head blight of winter wheat. *Appl. Environ. Microbiol.* 67:1575-1580.

Emms, D. M. and Kelly, S. 2019. OrthoFinder: phylogenetic orthology inference for comparative genomics. *Genome Biol*. 20:238.

Fischer, M. and Pleiss, J. 2003. The lipase engineering database: a navigation and analysis tool for protein families. *Nucleic Acids Res*. 31:319-321.

Flynn, J. M., Hubley, R., Goubert, C., Rosen, J., Clark, A. G., Feschotte, C. and Smit, A. F. 2020. RepeatModeler2 for automated genomic discovery of transposable element families. *Proc. Natl. Acad. Sci. U. S. A.* 117:9451-9457.

Gabriel, L., Brůna, T., Hoff, K. J., Ebel, M., Lomsadze, A., Borodovsky, M. and Stanke, M. 2024. BRAKER3: fully automated genome annotation using RNA-seq and protein evidence with GeneMark-ETP, AUGUSTUS, and TSEBRA. *Genome Res.* 34:769-777.

Gardes, M. and Bruns, T. D. 1993. Its primers with enhanced specificity for Basidiomycetes: application to the identification of mycorrhizae and rusts. *Mol. Ecol.* 2:113-118.

Hue, Y., Kim, J. H., Nam, Y., Choi, B., Kim, T. S., Lee, S.-J. and Kim, K.-T. 2025. Changes in the occurrence patterns of rice fungal diseases due to climate change. *Res. Plant Dis.* 31:17-29.

Jang, S.-H., Kim, S., Kim, S., Chung, H. and Park, S.-Y. 2024. Optimization of conditions for conidial production in *Bipolaris oryzae* isolated from rice. *Res. Plant Dis.* 30:229-235 (in Korean).

Kaboré, K. H., Kassankogno, A. I., Adreit, H., Milazzo, J., Guillou, S., Blondin, L., Chopin, L., Ravel, S., Charriat, F., Barro, M., Tollenaere, C., Lebrun, M.-H. and Tharreau, D. 2022. Genetic diversity and structure of *Bipolaris oryzae* and *Exserohilum rostratum* populations causing brown spot of rice in Burkina Faso based on genotyping-by-sequencing. *Front. Plant Sci.* 13:1022348.

Kaboré, K. H., Kassankogno, A. I. and Tharreau, D. 2025. Brown spot of rice: worldwide disease impact, phenotypic and genetic diversity of the causal pathogen *Bipolaris oryzae*, and management of the disease. *Plant Pathol.* 74:908-922.

Katoh, K. and Standley, D. M. 2013. MAFFT multiple sequence alignment software version 7: improvements in performance and usability. *Mol. Biol. Evol.* 30:772-780.

Kim, S., Chung, H., Jang, S.-H., Kim, S., Kim, K.-T. and Park, S.-Y. 2025. Random amplified polymorphic DNA-based analysis of genetic diversity and characterization of representative *Bipolaris oryzae* isolates from 2023-2024. *Plant Pathol. J.* 41:671-681.

Kolmogorov, M., Yuan, J., Lin, Y. and Pevzner, P. A. 2019. Assembly of long, error-prone reads using repeat graphs. *Nat. Biotechnol.* 37:540-546.

Li, H. 2013. Aligning sequence reads, clone sequences and assembly contigs with BWA-MEM. Preprint at arXiv: https://doi.org/10.48550/arXiv.1303.3997.

Liu, M., Yang, W., Gu, X., Xiao, Y., Yang, L., Zhang, Z., Wei, T., Hsiang, T., Zhang, Y. and Li, G. 2024. A nanopore-sequenced high-quality genome of the *Bipolaris oryzae* strain Bo-1. *Microbiol. Resour. Announc.* 13:e0038824.

Long, Y., Tang, T., Wang, L.-Y., He, B. and Gao, K. 2019. Absolute configuration and biological activities of meroterpenoids from an endophytic fungus of *Lycium barbarum*. *J. Nat. Prod.* 82:2229-2237.

Manamgoda, D. S., Rossman, A. Y., Castlebury, L. A., Crous, P. W., Madrid, H., Chukeatirote, E. and Hyde, K. D. 2014. The genus *Bipolaris*. *Stud. Mycol.* 79:221-288.

Manni, M., Berkeley, M. R., Seppey, M. and Zdobnov, E. M. 2021. BUSCO: assessing genomic data quality and beyond. *Curr. Protoc.* 1:e323.

Marçais, G., Delcher, A. L., Phillippy, A. M., Coston, R., Salzberg, S. L. and Zimin, A. 2018. MUMmer4: a fast and versatile genome alignment system. *PLoS Comput. Biol.* 14:e1005944.

Medd, R. W., Murray, G. M. and Pickering, D. I. 2003. Review of the epidemiology and economic importance of *Pyrenophora semeniperda*. *Australas. Plant Pathol.* 32:539-550.

Meshram, S., Gogoi, R., Bashyal, B. M., Kumar, A., Mandal, P. K. and Hossain, F. 2022. Comparative transcriptome analysis of fungal pathogen *Bipolaris maydis* to understand pathogenicity behavior on resistant and susceptible non-CMS maize genotypes. *Front. Microbiol.* 13:837056.

Moolhuijzen, P. M., Muria-Gonzalez, M. J., Syme, R., Rawlinson, C., See, P. T., Moffat, C. S. and Ellwood, S. R. 2020. Expansion and conservation of biosynthetic gene clusters in pathogenic *Pyrenophora* spp. *Toxins* 12:242.

Nunes, C. C. and Dean, R. A. 2012. Host-induced gene silencing: a tool for understanding fungal host interaction and for developing novel disease control strategies. *Mol. Plant Pathol.* 13:519-529.

Ouedraogo, I., Wonni, I., Sereme, D. and Kabore, K. B. 2016. Survey of fungal seed-borne diseases of rice in Burkina Faso. *Int. J. Agric. Innov. Res.* 5:476-480.

Price, M. N., Dehal, P. S. and Arkin, A. P. 2010. FastTree 2: approximately maximum-likelihood trees for large alignments. *PLoS ONE* 5:e9490.

Rawlings, N. D., Barrett, A. J. and Bateman, A. 2010. Merops: the peptidase database. *Nucleic Acids Res.* 38:D227-D233.

Sheng, P., Xu, M., Zheng, Z., Liu, X., Ma, W., Ding, T., Zhang, C., Chen, M., Zhang, M., Cheng, B. and Zhang, X. 2023. Peptidome and transcriptome analysis of plant peptides involved in *Bipolaris maydis* infection of maize. *Plants* 12:1307.

Song, X., Geng, Y., Xu, C., Li, J., Guo, Y., Shi, Y., Ma, Q., Li, Q. and Zhang, M. 2024. The complete mitochondrial genomes of five critical phytopathogenic *Bipolaris* species: features, evolution, and phylogeny. *IMA Fungus* 15:15.

Sperschneider, J. and Dodds, P. N. 2022. Effectorp 3.0: prediction of apoplastic and cytoplasmic effectors in fungi and oomycetes. *Mol. Plant-Microbe Interact.* 35:146-156.

Sunder, S., Singh, R. and Agarwal, R. 2014. Brown spot of rice: an overview. *Indian Phytopathol.* 67:201-215.

Terlouw, B. R., Blin, K., Navarro-Munoz, J. C., Avalon, N. E., Chevrette, M. G., Egbert, S., Lee, S., Meijer, D., Recchia, M. J. J., Reitz, Z. L van Santen, J. A., Selem-Mojica, N., Tørring, T., Zaroubi, L., Alanjary, M., Aleti, G., Aguilar, C., Al-Salihi, S. A. A., Augustijn, H. E., Avelar-Rivas, J. A., Avitia-Domínguez, L. A., Barona-Gómez, F., Bernaldo-Agüero, J., Bielinski, V. A., Biermann, F., Booth, T. J., Carrion Bravo, V. J., Castelo-Branco, R., Chagas, F. O., Cruz-Morales, P., Du, C., Duncan, K. R., Gavriilidou, A., Gayrard, D., Gutiérrez-García, K., Haslinger, K., Helfrich, E. J. N., van der Hooft, J. J. J., Jati, A. P., Kalkreuter, E., Kalyvas, N., Kang, K. B., Kautsar, S., Kim, W., Kunjapur, A. M., Li, Y.-X., Lin, G.-M., Loureiro, C., Louwen, J. J. R., Louwen, N. L. L., Lund, G., Parra, J., Philmus, B., Pourmohsenin, B., Pronk, L. J. U., Rego, A., Rex, D. A. B., Robinson, S., Rosas-Becerra, L. R., Roxborough, E. T., Schorn, M. A., Scobie, D. J., Singh, K. S., Sokolova, N., Tang, X., Udwary, D., Vigneshwari, A., Vind, K., Vromans, S. P. J. M., Waschulin, V., Williams, S. E., Winter, J. M., Witte, T. E., Xie, H., Yang, D., Yu, J., Zdouc, M., Zhong, Z., Collemare, J., Linington, R. G., Weber, T. and Medema, M. H. 2023. MIBiG 3.0: a community-driven effort to annotate experimentally validated biosynthetic gene clusters. *Nucleic Acids Res.* 51:D603-D610.

Teufel, F., Almagro Armenteros, J. J., Johansen, A. R., Gíslason, M. H., Pihl, S. I., Tsirigos, K. D., Winther, O., Brunak, S., von Heijne, G. and Nielsen, H. 2022. SignalP 6.0 predicts all five types of signal peptides using protein language models. *Nat. Biotechnol.* 40:1023-1025.

Vidhyasekaran, P., Borromeo, E. S. and Mew, T. W. 1986. Host-specific toxin production by *Helminthosporium oryzae*. *Phytopathology* 76:261-266.

Walker, B. J., Abeel, T., Shea, T., Priest, M., Abouelliel, A., Sakthikumar, S., Cuomo, C. A., Zeng, Q., Wortman, J., Young, S. K. and Earl, A. M. 2014. Pilon: an integrated tool for comprehensive microbial variant detection and genome assembly improvement. *PLoS ONE* 9:e112963.

White, T. J., Bruns, T., Lee, S. and Taylor, J. 1990. Amplification and direct sequencing of fungal ribosomal RNA genes for phylogenetics. In: *PCR protocols: a guide to methods and applications*, eds. by M. A. Innis, D. H. Gelfand, J. J. Sninsky and T. J. White, pp. 315-322. Academic Press, San Diego, CA, USA.

Wong, T. K. F., Ly-Trong, N., Ren, H., Baños, H., Roger, A. J., Susko, E., Bielow, C., De Maio, N., Goldman, N., Hahn, M. W., Huttley, G., Lanfear, R. and Minh, B. Q. 2025. IQ-TREE 3: Phylogenomic inference software using complex evolutionary models. Preprint at: https://doi.org/10.32942/X2P62N.

Xia, X., Wang, Y., Zhou, S., Liu, W. and Wu, H. 2022. Genome sequence resource for *Bipolaris zeicola*, the cause of northern corn leaf spot disease. *Phytopathology* 112:1192-1195.

Xiao, J. Z., Tsuda, M., Doke, N. and Nishimura, S. 1991. Phytotoxins produced by germinating spores of *Bipolaris oryzae*. *Phytopathology* 81:58-64.

Yan, J., Pang, J., Liang, J., Yu, W., Liao, X., Aobulikasimu, A., Yi, X., Yin, Y., Deng, Z. and Hong, K. 2022. The biosynthesis and transport of ophiobolins in *Aspergillus ustus* 094102. *Int. J. Mol. Sci.* 23:1903.

Zaccaron, A. Z. and Bluhm, B. H. 2017. The genome sequence of *Bipolaris cookei* reveals mechanisms of pathogenesis underlying target leaf spot of sorghum. *Sci. Rep.* 7:17217.

Zechmann, B. 2020. Subcellular roles of glutathione in mediating plant defense during biotic stress. *Plants* 9:1067.

Zhang, Y., Crous, P. W., Schoch, C. L. and Hyde, K. D. 2012. Pleosporales. *Fungal Divers.* 53:1-221.

Zheng, J., Ge, Q., Yan, Y., Zhang, X., Huang, L. and Yin, Y. 2023. dbCAN3: automated carbohydrate-active enzyme and substrate annotation. *Nucleic Acids Res.* 51:W115-W121.